

High-spin structures in ^{108}Pd : γ -vibrational band and two-quasineutron excitations

J. A. Alcántara-Núñez, J. R. B. Oliveira, E. W. Cybulska, N. H. Medina, M. N. Rao, R. V. Ribas, M. A. Rizzutto, W. A. Seale, F. Falla-Sotelo, and K. T. Wiedemann

Instituto de Física, Universidade de São Paulo, São Paulo, SP, Caixa Postal 66318, 05315-970, Brazil

(Received 2 December 2004; published 26 May 2005)

The high-spin structures of the ^{108}Pd nucleus have been studied with the $^{100}\text{Mo}(^{11}\text{B}, p2n\gamma)$ reaction at 43 MeV incident energy. γ - γ - t , γ - γ -charged-particle coincidences and directional correlation ratios were measured using the SACI-PERERE γ spectrometer formed by four Compton suppressed HPGe detectors and a 4π charged-particle ancillary detector system. Recent results for the γ -vibrational band and the $\nu h_{11/2} \otimes \nu(g_{7/2}, d_{5/2})$ negative parity structures have been confirmed and complemented. A new band tentatively based on the second lowest ($\nu h_{11/2}$) excitation has been observed.

DOI: 10.1103/PhysRevC.71.054315

PACS number(s): 21.10.Re, 23.20.En, 23.20.Lv, 27.60.+j

I. INTRODUCTION

The nuclei around $Z \sim 44$ and $N \sim 60$ are susceptible to dramatic changes in shape with the addition or subtraction of a small number of nucleons [1]. In the region of the Pd nuclei the rotational alignment of proton $g_{9/2}$ and neutron $h_{11/2}$ intruder orbitals can give rise to a significant increase in aligned angular momentum, resulting in a variety of collective behaviors. Previous experiments on $^{100-106}\text{Pd}$ nuclei show that the majority of states, populated by (HI, xn) reactions, are members of decoupled collective bands built on quasineutron states [2–4]. Similar characteristics can be also seen in the neighboring even Ru isotopes [5,6].

On the other hand, the nuclides in this mass region are known to have low-energy collective states which are well described as vibrational excitations, because they are near the $Z = 50$ shell closure. The structure of their lowest-lying states is dominated by vibrational degrees of freedom as reflected in the typical 0^+ , 2^+ , and 4^+ triplet of states, at about twice the energy of the first 2^+ state [7]. Furthermore, the total Routhian surface (TRS) calculation for the ^{108}Pd vacuum has shown, in the work of Pohl *et al.* (see Fig. 11 in Ref. [8]), a prolate minimum which is very soft along the β and γ parameters. This softness of the predicted minimum indicates vibrational behavior of this structure. Such characteristics can be illustrated through an empirical analysis (E-GOS), proposed by Regan *et al.* [9].

In this work, we present the results of an investigation of ^{108}Pd with the $^{100}\text{Mo}(^{11}\text{B}, p2n\gamma)$ reaction. Previous results [8,10], in particular a recent one obtained from an induced fission experiment in EUROBALL4 [11], have essentially been confirmed and complemented. New structures with rotational characteristics have been observed.

II. EXPERIMENTAL PROCEDURES

The high-spin states in the ^{108}Pd nucleus have been populated by the $^{100}\text{Mo}(^{11}\text{B}, p2n\gamma)$ reaction at 43 MeV beam energy. The beam was provided by the 8MV Pelletron Tandem accelerator of the University of São Paulo. The target used was an $\approx 18 \text{ mg/cm}^2$ metallic self-supporting foil of enriched ^{100}Mo

sufficiently thick in order to stop the recoils. γ rays and charged particles have been detected using the SACI-PERERE array. SACI [12] (Sistema Ancilar de Cintiladores) is a 4π charged particle telescope system consisting of 11 plastic phoswich scintillators, arranged in the geometry of a dodecahedron. Each telescope consists of a 0.1 mm thick fast scintillation (BC400, 2.4 ns) ΔE detector bonded to a 10 mm thick long decay time (BC444, 264 ns) E detector. The light-charged-particle detector array (SACI) enabled the selection of the evaporated charged particle fold in coincidence with the observed γ rays. PERERE [13] (Pequeno Espectrômetro de Radiação Eletromagnética com Rejeição de Espalhamento) is the γ -ray spectrometer consisting of 4 HPGe detectors with BGO Compton shields (two detectors were Ortec GMX of about 20% efficiency and the other two were Canberra REGe of 60% efficiency). Two of these detectors (one of each kind) were placed at 37° and the other two at 101° with respect to the beam direction. The total photopeak efficiency (around 1.3 MeV) of the system is about 0.5%. Events were collected on tape when at least two HPGe detectors fired in coincidence. The data were taken for a period of 136 h. A total of 85×10^6 Compton-suppressed events was collected. The data have been sorted into symmetrized total, α -gated, and p -gated γ - γ matrices with 1.7×10^8 , 2.5×10^6 , and 2.7×10^6 counts, respectively. The data were analysed using the VPAK [14] and RADWARE [15] spectrum analysis codes.

The main exit channels of the reaction are produced by the evaporation of three and four neutrons leading to $^{107,108}\text{Ag}$ isotopes [16,17]. The γ -ray transitions belonging to the $1\alpha 2n$ channel (^{105}Rh) were identified by setting gates on charged particle fold 1α [18]. The γ -ray transitions belonging to ^{108}Pd were identified by setting gates on charged particle fold $1p$ (see Fig. 1). γ rays from ^{107}Pd , which is another significant channel ($1p3n$) in the $1p$ gated spectra, were identified from previous work [8]. The assignment of the spins and parities to the ^{108}Pd levels was based on the DCO (directional correlation from oriented states) ratios. A γ - γ matrix was constructed by sorting the data from the two detectors positioned at 37° against the two detectors at 101° with respect to the beam direction. Gates were set on each axis on several strong quadrupole

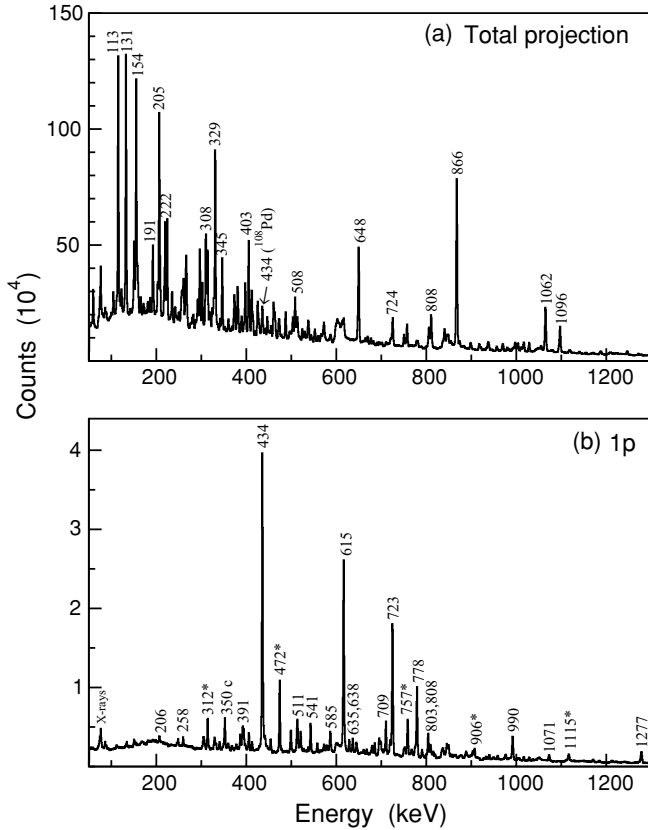


FIG. 1. γ -ray spectra (a) total projection and (b) gated with particle fold $1p$. In (a) most lines are from $^{107,108}\text{Ag}$ and in (b) from ^{108}Pd . The transitions marked with an asterisk belong to ^{107}Pd .

transitions and the intensity of other transitions observed in the two spectra has been extracted. $I_{\gamma}(37^{\circ})$ and $I_{\gamma}(101^{\circ})$ represent the intensity of a transition when gating on the 101° and 37° detector axes, respectively. The theoretical DCO ratios referred to a stretched quadrupole gate

$$R_{\text{DCO}} = \frac{I_{\gamma}(37^{\circ})}{I_{\gamma}(101^{\circ})},$$

obtained for the present geometry and reaction are $R_{\text{DCO}} = 1.0$ for quadrupole transitions and $R_{\text{DCO}} = 0.49$ for pure dipole transitions ($\Delta I = 1$). In the calculations, a state with initial spin of $20\hbar$ and a Gaussian distribution of magnetic substates with a standard deviation of $2.5\hbar$ was assumed. For mixed $E2/M1$ transitions, the DCO ratio varies with δ , with a maximum of 1.4 and a minimum of 0.2 for positive and negative mixing ratios, respectively (both for $|\delta| \approx 1$). The $\Delta I = 0$ transitions can give DCO ratios between 1.1 (the value for a pure dipole) and 0.44 (for large mixing ratios). These values are calculated assuming high spin states but are also valid for a stretched cascade feeding, down to low spins, whether gating above or below. However, when one or more mixed or unstretched transitions occur within the cascade, and the levels involved are at low spin, significant deviations from these general rules are to be expected and

detailed calculations have to be done for each specific case.

The stopping time of the recoils in the Mo target is estimated to be about 0.6 ps. Since no significant Doppler broadening was observed in any of the γ -ray lines assigned to ^{108}Pd , it can be inferred that the effective level lifetimes are at least a fraction of that time.

III. RESULTS

The level scheme of the ^{108}Pd nucleus deduced from the present work is shown in Fig. 2. This level scheme is based on the coincidence relationships, intensity balances for each level and energy sums from different paths using the $1p$ -gated matrix, and is essentially in agreement with earlier work [8,10], except for the placement of one 626 keV γ ray, previously assigned to a transition from a $I^{\pi} = (8^+)$ level at 2398 keV excitation energy to the $I^{\pi} = 6^+$ level of band 1. In our work, a γ ray of similar energy (627 keV) was placed in the middle of band 3b. This last structure, together with the γ -vibrational band (5a and 5b in Fig. 2) was also observed in Ref. [11]. The present results can be considered as a completely independent confirmation since they were obtained before that publication. Partial results of the present work have been published in conference proceedings [19], and the level scheme was presented in Ref. [20]. All the transitions reported in Ref. [11] are confirmed with exception of the 1092 and 581 keV transitions, from the level at 2864 keV excitation energy already known from the β decay of the high-spin isomer ^{108}Rh [21,22], which could not be observed in the present experiment. The 948 keV transition (from the 2283 keV level) intensity is quite small. This evidentiates a different population pattern by induced fission in comparison with fusion evaporation. In contrast, additional transitions were observed at the highest spins of most bands (one in each of bands 2, 5a, and 5b, and two in each of bands 3a and 3b). Band 4 and structures 3c and 3d were observed for the first time. A few transitions were also observed which were not classified into bands, and we have experimental results which allow for the spin assignment of several states.

The γ -ray energies and relative intensities of all the transitions assigned to ^{108}Pd are given in Table I, which also shows the DCO ratios and the resulting spin and parity assignments. The observed levels are grouped into five structures with rotational characteristics, labeled 1–5 in Fig. 2 for the purposes of discussion.

Band 1 is the yrast (up to $I^{\pi} = 8^+$) positive-parity band with the 0^+ ground state as the bandhead, and presents $E2$ transitions. In the present measurement, band 1 was observed up to spin $I^{\pi} = 14^+$. Band 2, also characterized by $E2$ transitions, was observed up to spin $I^{\pi} = 18^+$. This band is weakly populated by three new γ transitions of 863, 913, and 966 keV.

In band structure 3 we have observed transitions which can be considered to belong to the unfavored signature partner of band 3a, labeled as 3b in Fig. 2 and additional similar bandlike structures 3c and 3d. Band 3b was established above

TABLE I. γ -ray energy, initial and final excitation energy, spin and parity assignments, relative intensity, and DCO ratio for the transitions in ^{108}Pd . The relative intensities (normalized to 100 for the 614.6 keV transition) were obtained from the analysis of the $1p$ -gated matrix.

E_γ (keV)	E_i (keV)	E_f (keV)	$I_i^\pi \rightarrow I_f^\pi$	I_γ	R_{DCO}
132.8(3)	2842.9	2710.4	$7^- \rightarrow 6^{(-)}$	0.28(6)	
205.6(2)	2531.0	2325.2	$\rightarrow 5^-$	0.68(11)	0.80(24)
246.8(1)	3089.8	2842.9	$8^{(-)} \rightarrow 7^-$	0.96(10)	0.42(7)
258.3(1)	3101.1	2842.9	$8^{(-)} \rightarrow 7^-$	1.15(10)	0.43(8)
303.4(2)	3258.0	2954.5	$10^+ \rightarrow (8^+)$	0.39(6)	0.89(30)
313.1(9)	2084.3	1771.9	$5^+ \rightarrow 6^+$	0.68(14)	0.70(9)
327.7(1)	3089.8	2762.1	$8^{(-)} \rightarrow 7^-$	2.49(17)	0.55(14)
339.0(1)	3101.1	2762.1	$8^{(-)} \rightarrow 7^-$	1.87(14)	0.58(11)
373.6(14)	3794.6	3421.0	$10^{(-)} \rightarrow 9^-$	0.20(5)	
385.2(1)	2710.4	2325.2	$6^{(-)} \rightarrow 5^-$	2.76(20)	0.70(15)
390.7(1)	3101.1	2710.4	$8^{(-)} \rightarrow 6^{(-)}$	2.32(16)	0.81(20)
404.4(1)	1335.9	931.6	$3^+ \rightarrow 2^+$	3.85(26)	0.91(15)
434.1(1)	434.1	0.0	$2^+ \rightarrow 0^+$	122.1(10) ^a	0.97(5)
436.8(1)	2762.1	2325.2	$7^- \rightarrow 5^-$	2.66(20)	1.08(25)
439.4(2)	3111.2	2671.7	$(7^+) \rightarrow (5^+)$	0.81(15)	0.85(29)
497.4(1)	931.6	434.1	$2^+ \rightarrow 2^+$	10.5(6)	0.84(8) ^b
511.3(1)	2283.1	1771.9	$\rightarrow 6^+$	2.40(27)	
519.0(1)	3281.1	2762.1	$9^- \rightarrow 7^-$	7.05(33)	1.00(18)
525.4(1)	3287.5	2762.1		1.42(18)	
541.3(1)	3799.3	3258.0	$12^+ \rightarrow 10^+$	9.97(40)	1.09(11)
572.4(3)	3860.0	3287.5	$\rightarrow 7^-$	0.57(11)	
576.5(1)	1624.9	1048.6	$4^+ \rightarrow 4^+$	2.25(23)	
578.2(2)	3421.0	2842.9	$9^- \rightarrow 7^-$	0.86(14)	1.07(44)
614.6(1)	1048.4	434.1	$4^+ \rightarrow 2^+$	100.3(34)	0.99(5)
617.9(2)	1052.0	434.1	$0^+ \rightarrow 2^+$	4.0(5)	
627.1(1)	3728.2	3101.1	$10^{(-)} \rightarrow 8^{(-)}$	3.29(21)	0.84(21)
634.9(1)	2259.8	1624.9	$6^+ \rightarrow 4^+$	7.12(39)	1.18(27) ^b
637.8(2)	3749.0	3111.2	$(9^+) \rightarrow (7^+)$	0.80(13)	
659.0(2)	3421.0	2762.1	$9^- \rightarrow 7^-$	0.97(16)	0.94(26)
683.7(1)	3964.8	3281.1	$11^- \rightarrow 9^-$	4.01(23)	0.91(17)
693.3(1)	1624.9	931.6	$4^+ \rightarrow 2^+$	7.0(5)	1.49(24) ^{b,c}
694.7(1)	2954.5	2259.8	$(8^+) \rightarrow 6^+$	3.21(31)	1.49(24) ^{b,c}
704.8(2)	3794.6	3089.8	$10^{(-)} \rightarrow 8^{(-)}$	1.43(15)	
708.6(1)	3258.0	2549.4	$10^+ \rightarrow 8^+$	14.9(6)	1.05(11)
723.2(1)	1771.9	1048.6	$6^+ \rightarrow 4^+$	75.8(25)	0.97(5)
748.3(1)	2084.3	1335.9	$5^+ \rightarrow 3^+$	4.08(31)	1.42(30) ^b
757.2(2)	2529.1	1771.9	$\rightarrow 6^+$	1.73(26)	
765.5(1)	4493.8	3728.2	$12^{(-)} \rightarrow 10^{(-)}$	1.92(16)	0.82(15)
774.5(2)	4195.6	3421.0	$11^- \rightarrow 9^-$	1.45(20)	1.46(51)
777.6(1)	2549.4	1771.9	$8^+ \rightarrow 6^+$	40.1(14)	0.97(7)
780.0(9)	4529.0	3749.0	$(11^+) \rightarrow (9^+)$	0.28(12)	
802.5(1)	3351.9	2549.4	$10^+ \rightarrow 8^+$	13.2(5)	0.98(10)
807.7(1)	4159.6	3351.9	$12^+ \rightarrow 10^+$	5.48(28)	0.97(12)
813.8(1)	4778.6	3964.8	$13^- \rightarrow 11^-$	2.11(16)	0.91(15)
818.0(1)	4977.5	4159.6	$14^+ \rightarrow 12^+$	1.72(16)	0.99(20)
832.9(2)	5326.6	4493.8	$(14^-) \rightarrow 12^{(-)}$	1.07(12)	
835.0(2)	2919.3	2084.3	$(7^+) \rightarrow 5^+$	1.50(20)	
836.3(3)	3790.7	2954.5	$(10^+) \rightarrow (8^+)$	0.57(12)	
842.4(11)	5371.4	4529.0	$(13^+) \rightarrow (11^+)$	0.26(11)	
844.1(1)	4643.4	3799.3	$14^+ \rightarrow 12^+$	4.95(25)	0.93(19)
847.6(4)	2472.5	1624.9	$\rightarrow 4^+$	0.82(20)	
854.2(2)	5632.8	4778.6	$15^- \rightarrow 13^-$	0.76(11)	0.85(23)
863.4(3)	4121.4	3258.0	$(11) \rightarrow 10^+$	0.86(15)	0.67(23)

TABLE I. (Continued.)

E_γ (keV)	E_i (keV)	E_f (keV)	$I_i^\pi \rightarrow I_f^\pi$	I_γ	R_{DCO}
875.4(3)	3424.8	2549.4	$\rightarrow 8^+$	0.93(18)	
885.3(3)	6518.1	5632.8	$(17^-) \rightarrow 15^-$	0.40(9)	
890.6(4)	4685.2	3794.6	$(12^-) \rightarrow 10^{(-)}$	0.36(10)	
897.1(4)	5609.1	4711.9	$\rightarrow (13)$	0.39(10)	
899.4(8)	6226.0	5326.6	$(16^-) \rightarrow (14^-)$	0.24(13)	
901.8(1)	1335.9	434.1	$3^+ \rightarrow 2^+$	6.1(5)	0.94(16) ^b
912.5(2)	4711.9	3799.3	$(13) \rightarrow 12^+$	0.88(13)	0.65(15)
931.7(2)	931.6	0.0	$2^+ \rightarrow 0^+$	2.14(31)	0.92(26)
938.2(1)	2710.4	1771.9	$6^{(-)} \rightarrow 6^+$	2.64(23)	1.33(30)
947.9(2)	2283.7	1335.9	$\rightarrow 3^+$	1.40(24)	
966.1(6)	5609.1	4643.4	$\rightarrow 14^+$	0.35(13)	
973.8(2)	5133.3	4159.6	$\rightarrow 12^+$	1.02(14)	
990.2(1)	2762.1	1771.9	$7^- \rightarrow 6^+$	15.4(7)	0.53(8)
1026.8(2)	4378.7	3351.9	$(11) \rightarrow 10^+$	0.99(16)	0.57(26)
1049.5(1)	5693.3	4643.4	$16^+ \rightarrow 14^+$	1.32(13)	0.88(23)
1070.9(1)	2842.9	1771.9	$7^- \rightarrow 6^+$	4.69(33)	0.51(10)
1136.0(10)	6829.3	5693.3	$18^+ \rightarrow 16^+$	0.41(10)	0.90(26)
1182.9(5)	2231.6	1048.6	$\rightarrow 4^+$	0.85(25)	
1211.2(5)	2259.8	1048.6	$6^+ \rightarrow 4^+$	0.77(21)	
1234.4(9)	2283.7	1048.6	$\rightarrow 4^+$	0.43(23)	
1240.7(5)	3790.7	2549.4	$(10^+) \rightarrow 8^+$	0.49(16)	
1276.6(1)	2325.2	1048.6	$5^- \rightarrow 4^+$	9.1(6)	0.58(9)
1482.9(4)	2531.0	1048.6	$\rightarrow 4^+$	1.18(26)	
1613.7(5)	2047.8	434.1	$3^- \rightarrow 2^+$	1.19(35)	
1623.1(2)	2671.7	1048.6	$(5^+) \rightarrow 4^+$	1.00(18)	

^aSum of the intensities of the transitions feeding the 2^+ level.

^bObtained from the 434 keV gate (see text).

^cFrom the sum of the 693 and 695 keV peak areas. Separate evaluations would lead to less reliable 1.80(33) and 1.09(30) values, respectively.

$\delta \leq -5$ (or $\delta \leq 0.2$ for the less likely positive mixing ratio solution). The theoretical values of the DCO ratios for band 5a, from the 434 keV gate have to be calculated considering the presence of the unstretched 497 keV transition from $2^+ \rightarrow 2^+$ within the cascade. Assuming the value of $\delta = -3.1$ for this transition one should expect the values of $R_{\text{DCO}} = 1.56$ for the quadrupole transitions and $R_{\text{DCO}} = 0.82$ for stretched dipoles. Indeed, although with rather large uncertainties, the experimental values for the quadrupole transitions of band 5 and for the 404 keV dipole ($3^+ \rightarrow 2^+$) are consistent with this prediction, allowing for the assignment of $I^\pi = 3^+$ for the level at 1336 keV in excitation. The tentative assignments presented in [11] are therefore confirmed, and, in addition, both even and odd-spin components (5a and 5b) of the band have been extended by one transition.

Figure 3 shows sums of clean gates for the bands labeled as 3b, 3c, 3d, 4, and 5. The transitions of 976 keV and a small part of the peak at 990 keV belong to ^{25}Mg which is formed by the reaction of ^{11}B with ^{16}O contaminant present on the target. They leak into the 833 keV gate due to the Doppler broadened 837 keV transition (the three transitions, 837, 990, and 976 keV, form a coincident cascade in ^{25}Mg). The transition marked with “c” is an unidentified contaminant.

IV. DISCUSSION

The experimental Routhians e' and alignments i , shown in Fig. 4 as a function of rotational frequency ($\hbar\omega$), were calculated according to the standard procedure described in Ref. [26,27], with the Harris parametrization of the moment of inertia: $\mathcal{J}_0 = 6\hbar^2 \text{MeV}^{-1}$ and $\mathcal{J}_1 = 20\hbar^4 \text{MeV}^{-3}$, taken from previous work [8]. The quasiparticle Routhians based on a deformed Woods-Saxon potential, including pairing interaction [28] calculated for $Z = 46$ and $N = 62$, are shown in Fig. 5. The deformation ($\beta_2 = 0.18$, $\beta_4 = 0.0$, $\gamma = 0^\circ$) and pairing-gap parameters used were chosen in accordance with the total Routhian surface (TRS) calculations [28,29] for the vacuum configuration (Fig. 6). The lowest quasiproton energy levels of positive parity ($g_{9/2}$) are labeled A , B , C , and D ; and those of negative parity ($1/2^- [301]$), E and F . For the neutrons, the first available $h_{11/2}$ orbitals are e , f , g , and h and for ($g_{7/2}$, $d_{5/2}$), a , b , c , and d .

A. The positive parity bands

In the present measurement, band 1 was observed up to $I^\pi = 14^+$. The aligned angular momentum increases up to the value $i \sim 10\hbar$ at a rotational frequency of $\hbar\omega \approx 0.4 \text{ MeV}$ (see

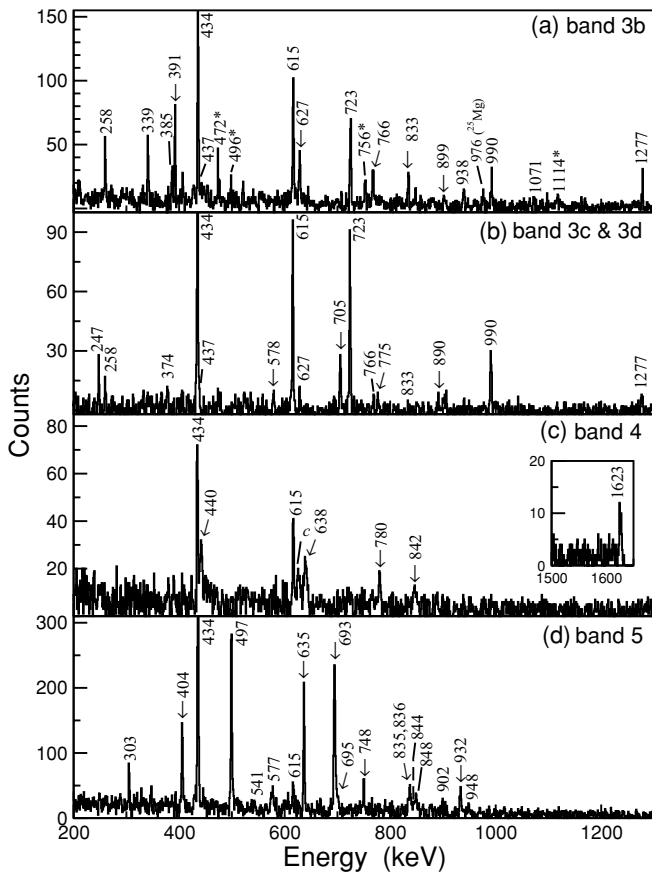


FIG. 3. γ -ray spectra from the $1p$ gated matrix. Sum of gates on (a) 627, 766, and 833 keV transitions belonging to band 3b, (b) 328 and 1071 transitions deexciting bands 3c and 3d, (c) 439, 638, and 1623 keV transitions belonging to band 4, (d) 404, 497, 635, 693, 695, and 748 keV transitions belonging to band 5, in ^{108}Pd . The transitions marked with an asterisk belong to ^{107}Pd .

Fig. 4). This enhancement of the i values is due to the evolution from vibrational structures to rotational structures present in nuclei in the $A \approx 110$ and $Z \approx 50$ region, as shown in the work of Regan *et al.* [9]. They illustrated this phenomenon by means of the E-GOS curves for the yrast sequence in ^{102}Ru and surrounding neighborhood compared with the perfect harmonic vibrator and the axially symmetric rotor (see Figs. 1 and 3 of Ref. [9]). Band 2 presents a gain in alignment of $\sim 10\hbar$ with relation to the beginning of band 1, corresponding to an alignment of the first two $h_{11/2}$ quasineutrons (ef). The two bands cross at $\hbar\omega \approx 0.35$ MeV.

The band labeled 4 in Fig. 2 was observed for the first time in the present work. The behavior of the alignment as a function of spin for this band resembles that of band 3 but is about $1.5\hbar$ units lower. There is no indication of a $vh_{11/2}^2$ low frequency crossing (at $\hbar\omega \approx 0.3$ MeV) as would be expected for a two-quasiproton configuration, so this possibility was considered unlikely. The next two-quasineutron configuration in excitation energy is eg (the second excited $vh_{11/2}^2$ configuration) with signature $\alpha = 1$, according to the CSM calculations, for which the $ef(vh_{11/2}^2)$ crossing is blocked. The experimental

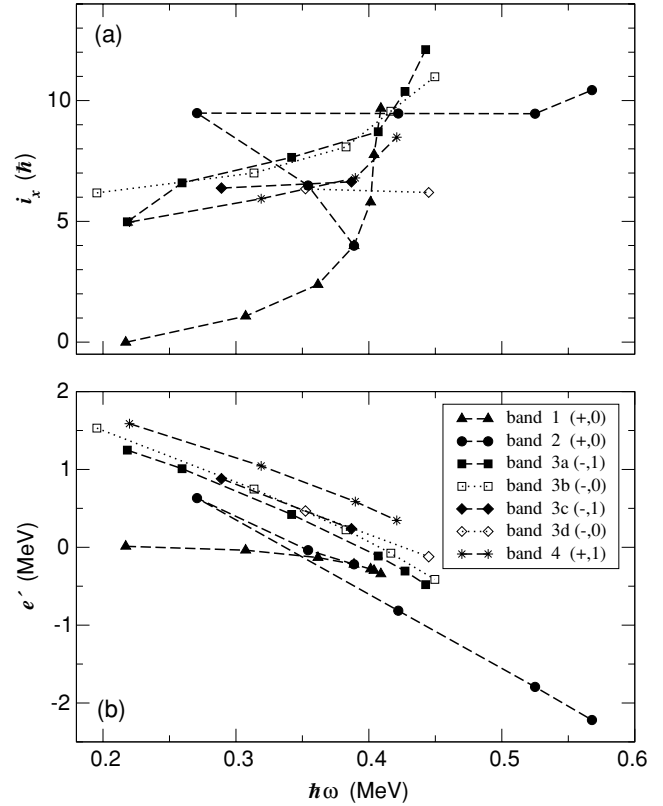


FIG. 4. Experimental quasiparticle (a) alignments and (b) Routhians as a function of the rotational frequency $\hbar\omega$ for the rotational bands in ^{108}Pd . The symbols correspond to the numbering of the bands and parity, signature (π, α) as indicated in the bottom panel.

alignments for this band, with the assumption of a $I^\pi = (5^+)$ state as a bandhead [see Fig. 4(a)], are around $i_x \approx 6\hbar$, in agreement with the CSM calculation for the quasineutron eg configuration. For these reasons we tentatively assign this configuration to band 4.

Band 5 is assigned as the γ -vibrational band. The bandhead is the second 2^+ state belonging to the two phonon triplet ($0^+, 2^+, 4^+$) of the purely vibrational model. Bands with similar characteristics were observed in the $A = 104$ to 108 even Ru isotopes in the work of Deloncle *et al.* [6] where, with the use of perturbation theory (see Ref. [30]), it was possible to organize the eigenstates into collective bands, ground-state, and γ -vibrational band. This solution for the four isotopes was given in Fig. 9 of Ref. [6]. On the other hand, Venkova *et al.* [31] present the potential energy surface (PES) for the ground states of $^{106,108,110}\text{Pd}$ nuclei calculated using a microscopic self-consistent model [32], which indicates that these isotopes exhibit a prolate shape ($\gamma \sim 0^\circ$) with triaxial softness increasing with the neutron number. This statement is in agreement with our TRS calculations for the vacuum of $^{102,104,106,108}\text{Pd}$ nuclei [20] where the position of the minima of deformation increase from an axial symmetry shape with $\gamma = 0^\circ$ to nearly $\gamma = 5^\circ$ as a function of the neutron number. The energy dependence of the first excited states of the yrast band and the side bands in even Pd isotopes, as a function

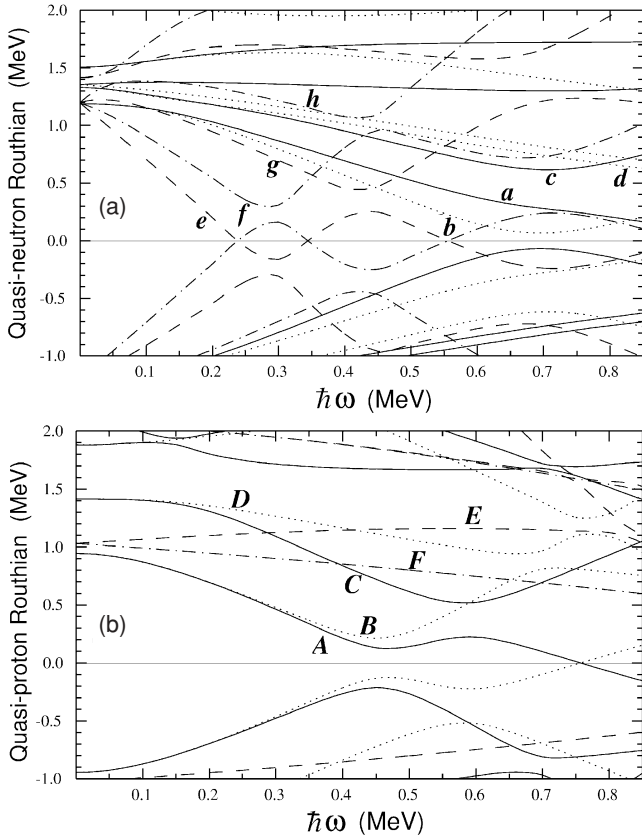


FIG. 5. Quasiparticle Routhians as a function of the rotational frequency $\hbar\omega$ for (a) neutrons and (b) protons, calculated at $\beta_2 = 0.18$, $\beta_4 = 0$, and $\gamma = 0^\circ$ for ^{108}Pd . The following convention is used for the levels: solid line ($\pi = +, \alpha = +1/2$), dotted line ($\pi = +, \alpha = -1/2$), dot-dashed line ($\pi = -, \alpha = +1/2$), and dashed line ($\pi = -, \alpha = -1/2$). The quasiparticle states are labeled by letters.

of neutron number [see Fig. 7(b)], is similar to the energy dependence of the first excited states of the yrast band and the side bands in even Ru isotopes, as shown in Fig. 7(a). Although both components of band 5 have been extended, no indication of a backbend has been observed up to the maximum frequency of about 0.42 MeV. If the effect exists, as expected, it appears to be delayed with comparison to the neighboring neutron rich isotopes [11].

B. The negative parity band structure

In the present work we have observed four interrelated bands (structure 3) with negative parity. Experimentally, bands 3a and 3b present an aligned angular momentum i of about $7\hbar$ and signature splitting $\Delta e' \approx 100$ keV (see Fig. 4), while 3c and 3d present somewhat smaller alignment and no signature splitting. The quasiparticle Routhians, calculated with the CSM, show that the eb configuration [essentially from $\nu h_{11/2} \otimes \nu(g_{7/2}, d_{5/2})$], has a low excitation energy (for two quasineutrons) and presents $\alpha = 1$ as a favored signature, i.e., states with odd spins (band 3a). This configuration presents an

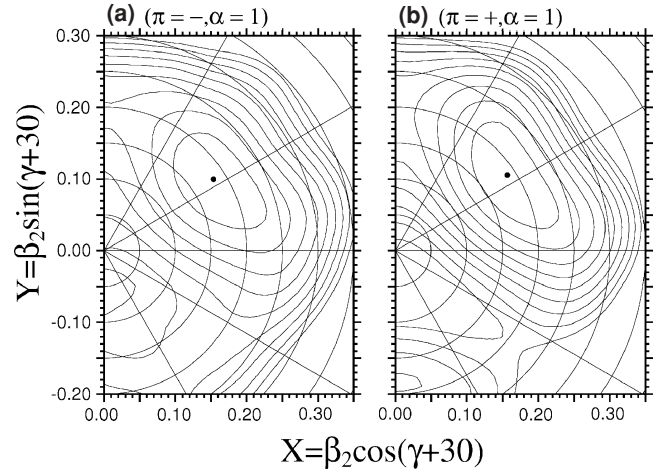


FIG. 6. Total Routhian surface calculations $\hbar\omega = 0.25$ MeV. (a) $\nu h_{11/2} \otimes (g_{7/2}, d_{5/2})$ configuration (eb); and (b) excited ($\nu h_{11/2}$)² configuration (eg) in ^{108}Pd . The thick dot indicates the position of the equilibrium deformation.

aligned angular momentum $i_x \approx 8\hbar$ with a signature splitting $\Delta e' \approx 150$ keV (between ea and eb) at a rotational frequency of $\hbar\omega \approx 0.4$ MeV. The four lowest (a, b, c , and d) positive parity orbitals from $(g_{7/2}, d_{5/2})$ are close in excitation energy, and combined with the lowest quasiparticle orbital e from $h_{11/2}$ configurations provide a possible explanation for the family of bands 3a–d. For this type of configuration the first quasineutron crossing, ef , is blocked, however, the first proton crossing AB , i.e. $\pi g_{9/2}^2$ (at $\hbar\omega \approx 0.5$ MeV) is possible. These statements are in reasonable agreement with the experimental alignments and Routhians for bands 3a–d. TRS calculations, for the eb configuration [see Fig. 6(a)], predict nearly axial symmetry with $\beta_2 \approx 0.19$ and $\gamma \approx 4^\circ$ (and similar results for the other combinations). The systematics of the bands of the $A = 102$ to 106 even Pd isotopes [5], and in the $A = 102$ to 106 even Ru isotopes [2,6] also show agreement with the assumption of the $\nu h_{11/2} \otimes \nu(g_{7/2}, d_{5/2})$ configuration for band structure 3.

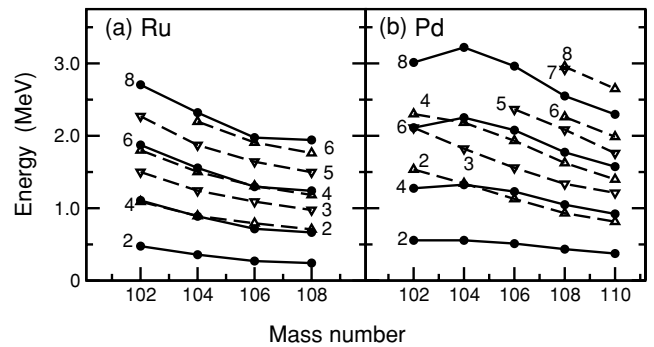


FIG. 7. First excited states of (a) $^{102,104,106,108}\text{Ru}$ and (b) $^{102,104,106,108,110}\text{Pd}$. Ground-state band (filled circles) and γ -vibrational band (empty triangles).

V. CONCLUSIONS

The high spin-states of the nucleus of ^{108}Pd have been measured and complemented. The γ -vibrational band has been confirmed and extended. The unfavored signature of the $\nu h_{11/2}(g_{7/2}, d_{5/2})$ negative parity configuration with two other closely related structures, and one new structure with low intensity, tentatively based on the second excited ($\nu h_{11/2}$) configuration, were interpreted within the cranking model framework.

ACKNOWLEDGMENTS

We thank the technical staff of the Pelletron Tandem Accelerator of the University of São Paulo. This work was partially supported by the Fundação de Amparo à Pesquisa do Estado de São Paulo (FAPESP) and the Conselho Nacional de Desenvolvimento Científico e Tecnológico (CNPq), Brazil.

-
- [1] *Nuclear Structure of the Zirconium Region*, edited by J. Eberth, R. Meyer, and K. Sistemich (Springer-Verlag, Berlin, 1988).
- [2] J. A. Grau, L. E. Samuelson, F. A. Rickey, P. C. Simms, and G. J. Smith, *Phys. Rev. C* **14**, 2297 (1976).
- [3] Dan Jerrestam, W. Klamra, B. Fogelberg, R. Bark, A. Gizon, J. Gizon, E. Iddeguchi, S. Mitarai, M. Piirinen, and G. Sletten, *Nucl. Phys.* **A603**, 203 (1996).
- [4] G. E. Perez, D. Sohler, A. Algora, Zs. Dombradi, B. M. Nyako, J. Timar, L. Zolnai, R. Wyss, J. Cederkall, A. Johnson, A. Kerek, W. Klamra, L.-O. Norlin, M. Lipoglavsek, C. Fahlander, A. Likar, M. Palacz, A. Atac, J. Nyberg, J. Persson, A. Gizon, J. Gizon, A. J. Boston, E. S. Paul, H. Grawe, R. Schubart, D. T. Joss, S. Juutinen, E. Makela, J. Kownacki, M. de Poli, P. Bednarczyk, G. de Angelis, D. Seweryniak, D. Foltescu, H.A. Roth, O. Skeppstedt, D. Jerrestam, T. Shizuma, G. Sletten, and S. Tormanen, *Nucl. Phys.* **A686**, 41 (2001).
- [5] H. Dejbakhsh and S. Bouttchenko, *Phys. Rev. C* **52**, 1810 (1995).
- [6] I. Deloncle, A. Bauchet, M.-G. Porquet, M. Girod, S. Peru, J.-P. Delaroche, A. Wilson, B. J. P. Gall, F. Hollinger, N. Schulz, E. Gueorgieva, A. Minkova, T. Kutsarova, Ts. Venkova, J. Duprat, H. Sergoller, C. Gautherin, R. Lucas, A. Astier, N. Buform, M. Meyer, S. Perries, and N. Redon, *Eur. Phys. J. A* **8**, 177 (2000).
- [7] L. E. Svensson, C. Fahlander, L. Hasselgren, A. Bäcklin, L. Westerberg, D. Cline, T. Czornyka, C. Y. Wu, R. M. Diamond, and H. Klue, *Nucl. Phys.* **A584**, 547 (1995).
- [8] K. R. Pohl, P. H. Regan, J. E. Bush, P. E. Raines, D. P. Balamuth, D. Ward, A. Galindo-Uribarri, V. P. Janzen, S. M. Mullins, and S. Pilotte, *Phys. Rev. C* **53**, 2682 (1996).
- [9] P. H. Regan *et al.*, *Phys. Rev. Lett.* **90**, 152502 (2003).
- [10] P. H. Regan, T. M. Menezes, C. J. Pearson, W. Gelletly, C. S. Purry, P. M. Walker, S. Juutinen, R. Julin, K. Helariutta, A. Savelius, P. Jones, P. Jämsen, M. Muikku, P. A. Butler, G. Jones, P. Greenlees, *Phys. Rev. C* **55**, 2305 (1997).
- [11] S. Lalkovski, A. Minkova, M.-G. Porquet, A. Bauchet, I. Deloncle, A. Astier, N. Buform, L. Donadille, O. Dorvaux, B.P. J. Gall, R. Lucas, M. Meyer, A. Prst, N. Redon, N. Schultz, and O. Stwsky, *Eur. Phys. J. A* **18**, 589 (2003).
- [12] J. A. Alcántara-Núñez, J. R. B. Oliveira, E. W. Cybulska, N. H. Medina, M. N. Rao, R. V. Ribas, M. A. Rizzutto, W. A. Seale, F. Falla-Sotelo, F. R. Espinoza-Quis, and C. Tenreiro, *Nucl. Instrum. Methods Phys. Res. A* **497**, 429 (2003).
- [13] R. V. Ribas, J. R. B. Oliveira, E. W. Cybulska, M. N. Rao, W. A. Seale, M. A. Rizzutto, and N. H. Medina, Annual Report of the Nuclear Physics Department, Institute of Physics, University of São Paulo, 1996, p. 63.
- [14] W. T. Milner, Holifield Heavy Ion Research Facility Computer Handbook, Oak Ridge National Laboratory, Oak Ridge, Tennessee, USA, 1987.
- [15] D. Radford, *Nucl. Instrum. Methods Phys. Res. A* **361**, 297 (1995).
- [16] F. R. Espinoza-Quiñones, E. W. Cybulska, J. R. B. Oliveira, R. V. Ribas, N. H. Medina, M. N. Rao, M. A. Rizzutto, L. G. R. Emediato, W. A. Seale, and S. Botelho, *Phys. Rev. C* **55**, 1548 (1997).
- [17] F. R. Espinoza-Quiñones *et al.*, *Phys. Rev. C* **52**, 104 (1995).
- [18] J. A. Alcántara-Núñez, J. R. B. Oliveira, E. W. Cybulska, N. H. Medina, M. N. Rao, R. V. Ribas, M. A. Rizzutto, W. A. Seale, F. Falla-Sotelo, K. T. Wiedemann, V. I. Dimitrov, and S. Frauendorf, *Phys. Rev. C* **69**, 024317 (2004).
- [19] J. A. Alcántara-Núñez, J. R. B. Oliveira, E. W. Cybulska, N. H. Medina, M. N. Rao, R. V. Ribas, M. A. Rizzutto, W. A. Seale, and F. Falla-Sotelo, *Braz. J. Phys.* **34**, 1005 (2004).
- [20] J. A. Alcántara-Núñez, Estruturas rotacionais quadrupolares elétricas e dipolares magnéticas nos núcleos de ^{105}Rh e ^{108}Pd , Instituto de Física, Universidade de São Paulo, Ph.D. thesis (2003).
- [21] J. A. Pinston, F. Schussler, and A. Moussa, *Nucl. Phys.* **A133**, 124 (1969).
- [22] P. Bhattacharya, *Nuovo Cimento A* **79**, 471 (1984).
- [23] Table of Isotopes, CD-Rom edition, edited by R. B. Firestone and V. S. Shirley (Wiley-Interscience, New York, 1996).
- [24] K. S. Krane, *Phys. Rev. C* **8**, 1494 (1973).
- [25] K. S. Krane and R. M. Steffen, *Phys. Rev. C* **2**, 724 (1970).
- [26] R. Bengtsson and S. Frauendorf, *Nucl. Phys.* **A327**, 139 (1979).
- [27] F. Döna and S. Frauendorf, *Proceedings of the International Conference on High Spin Properties of Nuclei, Oak Ridge*; N. R. Johnson, Harwood, *Nucl. Sci. Res. Ser.* **4**, 143 (1982).
- [28] R. Wyss, J. Nyberg, A. Johnson, R. Bengtsson, and W. Nazarewicz, *Phys. Lett.* **B215**, 211 (1988).
- [29] W. Nazarewicz, J. Dudek, R. Bengtsson, T. Bengtsson, and I. Ragnarsson, *Nucl. Phys.* **A435**, 397 (1985).
- [30] M. Girod and B. Grammaticos, *Nucl. Phys.* **A330**, 40 (1979).
- [31] Ts. Venkova, M.-G. Porquet, I. Deloncle, B. J. P. Gall, H. De Witte, P. Petkov, A. Bauchet, T. Kutsarova, E. Gueorgieva, J. Duprat, C. Gautherin, F. Hoellinger, R. Lucas, A. Minkova, N. Schulz, H. Sergolle, E. A. Stefanova, and A. Wilson, *Eur. Phys. J. A* **6**, 405 (1999).
- [32] B. Gall, P. Bonche, J. Dobaczewski, and H. Flocard, *Z. Phys. A* **348**, 187 (1994).